INTERNATIONAL JOURNAL OF PRECISION ENGINEERING AND MANUFACTURING Vol. 16, No. 4, pp. 629-637 APRIL 2015 / 629
DOI: 10.1007/s12541-015-0084-3 ISSN 2234-7593 (Print) / ISSN 2005-4602 (Online)

Material Removal of Glass by Magnetorheological Fluid Jet

Wook-Bae Kim[1,#], Eunseok Nam[2], Byung-Kwon Min[2], Doo-Sun Choi[3], Tae-Jin Je[3], and Eun-Chae Jeon[3]

1 Department of Mechanical Design Engineering, Korea Polytechnic University, 237, Sangidaehak-ro, Siheung-si, Gyeonggi-do, 429-793, South Korea
2 School of Mechanical Engineering, Yonsei University, 50, Yonsei-ro, Seodaemun-gu, Seoul, 120-749, South Korea
3 Nano-Convergence Mechanical Systems Research Division, Korea Institute of Machinery and Materials (KIMM), Daejeon, 305-343, South Korea
Corresponding Author / E-mail: wkim@kpu.ac.kr, TEL: +82-31-8041-0430, FAX: +82-2-8041-0439

KEYWORDS: Glass, Granular flow, Magnetorheological fluid jet, Polishing, Surface finishing, Surface roughness

Magnetorheological (MR) fluid jet polishing is a material removal process for precision products such as optical elements. It is characterized by a jet flow that is stabilized by a magnetic field, and a highly predictable machining spot. The behavior of the particles in an MR fluid slurry near a target wall surface is conceptually described. In experiments with a BK7 glass specimen, various removal spots are created by impingement of MR fluid jets at velocities of 10~30 m/s, using MR fluids of different compositions, and different processing durations. The tangential MR fluid flow along the part surface is assumed to be responsible for material removal, and theoretical models for the prediction of material removal are developed, using the conventional wear model and granular flow theory. The constitutive relation between the shear stress and the shear rate changes as the jet velocity increases, which has a critical effect on the behavior of material removal. CFD analysis is performed to calculate the wall shear rate. The proposed models agree with the experimental results with respect to the distribution of the material removal rate. Additionally, the surface topographies of polished parts are discussed, with regards to the particle behavior.

Manuscript received: July 23, 2014 / Revised: December 11, 2014 / Accepted: December 23, 2014

1. Introduction

The removal of materials by the impingement of fine abrasives or abrasive slurries is used in various precision, micromachining, and nanomachining methods, such as powder blasting, abrasive jet machining, and fluid jet polishing.[1-3] In the surface finishing field, these material removal processes are required because of the increasing demand for high-precision functional parts, and the high efficiency processes that these parts enable. In comparison to some other conventional polishing techniques, such as chemical-mechanical polishing, a particle jet or slurry jet does not require any specially shaped tools, and can also be applied to a complex curved surface.

These material removal processes are based on erosion phenomena that are often encountered in other industrial contexts as a serious problem. An extensive body of research has been produced on erosion behavior under various conditions. For single particle impact erosion, the impact angle, particle kinetic energy, and material properties (e.g. brittleness and ductility) are regarded as critical parameters.[4-8] From the machining point of view, the material removal rate and the final surface roughness, which are the essential performance criteria for precision polishing, depend on the erosion parameters with respect to the process and materials. However, it is difficult to achieve both a low surface roughness and a high material removal rate at the same time in an erosion mechanism. In the case of particle impact onto a flat surface at an arbitrary angle, as the kinetic energy of the particles increases the induced crater volume increases, resulting in a higher material removal rate, but deeper surface craters and greater surface roughness. Conversely, as the kinetic energy decreases the craters become smaller, and finally below the elastic-plastic threshold the particles have no lasting effect on the material.[9,10]

One promising approach for erosion-based fine finishing, with the objective of a high material removal rate and low surface roughness, is to apply a slurry jet with a high particle concentration but low kinetic energy. This allows a large number of particles to participate in material removal.[11,12] Magnetorheological (MR) fluid jet finishing, which was proposed by Kordonski et al, is a typical example of this approach, using a high particle concentration slurry (MR fluid) for fine polishing of optical glass.[13,14] An important feature of an MR fluid jet is its collimated jet stream. Whereas a common water-based slurry jet becomes disturbed by the surrounding air and spreads out as it travels,

the MR fluid jet from a nozzle is highly collimated and stable during traveling, until it impinges upon a workpiece. This behavior is due to the application of a strong magnetic field at the nozzle exit that causes an instantaneous increase in the fluid viscosity. The MR fluid jet results in predictable and consistent material removal spots on a workpiece surface, and therefore it can be used to correct the surface shape of a high precision optical element, following an estimation of the quantity of material to be removed.

However, a deeper understanding of the material removal mechanism and characteristics is necessary for wider application of MR fluid jets, or other slurry jets with high solid concentrations. Although there have been many investigations into the removal mechanisms of the fine finishing processes that use an MR fluid as a flexible tool,[15-19] these relate to the situation where an external magnetic field is applied near the part surface, and not at the nozzle to form a collimated jet. This results in a different material behavior. In these investigations the MR fluid is modeled as a flexible polishing lap whose stiffness can be controlled by an magnetic field.

The material removal mechanism during powder blasting and with low-concentration slurry jets, such as fluid jet polishing, has been modeled by the impact of single independent particles that are entrained along the fluid streamlines in many studies.[20,21] However, MR fluid is a high-concentration slurry with over 30 vol% of iron-based particles. The MR fluid jet will demonstrate a different material behavior than the conventional slurry jet.

In this study, the material removal characteristics of an MR fluid jet are investigated. The material removal profiles and the surface roughness of a glass surface are analyzed, based on both experiments and theoretical modeling. In particular, we propose that material removal is caused by the sliding friction of the MR fluid slurry over the part surface at limited jet velocities. The dynamic behavior of the particles in the MR fluid and the stress on the target surface are considered for the material removal modeling, assisted by granular flow theory.

2. Experiments

2.1 Apparatus and materials

A schematic of the MR jet polishing system is shown in Fig. 1. A workpiece of borosilicate crown glass BK7 (specific gravity: 2.51, Young's modulus: 82 GPa, Vickers microhardness: 5.2-7.5 GPa, nanohardness: 7.7 GPa), is mounted on a fixed table in a container with a drain connected to a reservoir. The slurry in the reservoir enters the inlet port of a diaphragm pump, and the pressurized slurry is then delivered to a steel nozzle located in the center of a cylindrical electromagnet. At the nozzle exit, the MR fluid is exposed to a magnetic field (field strength of 0.25T), which markedly increases the apparent viscosity of the slurry and stabilizes the jet. The influence of the magnetic field does not extend to near the workpiece. The inner diameter of the nozzle is 2 mm, and the distance between the nozzle and the surface of the workpiece is 40 mm. The flow pressure provided by the pump is continuously monitored by a pressure sensor.

Carbonyl iron powder is the most widely used magnetic component in MR fluids, and in general some additional abrasives are added for polishing applications. Three MR fluids were prepared, including a

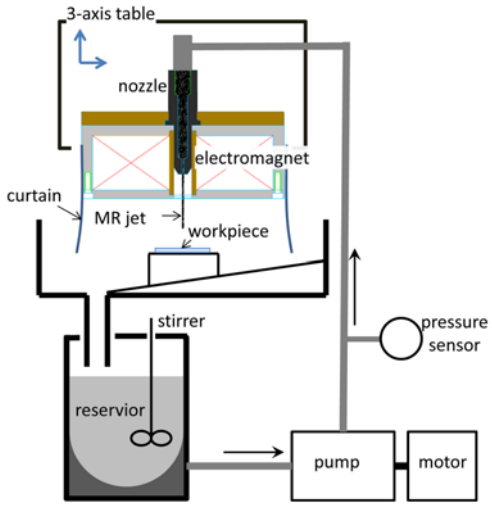

Fig. 1 Schematic of experimental setup

Table 1 Properties of two grades of CI particles

Mechanical grade (Model/manufacturer)	Soft grade (CC/Basf)	Hard grade (S-1640/ISP)
D50 diameter	3.8-5.3 μm	3.0-5.0 μm
Contents	Fe > 99.5%, C < 0.05%, N < 0.01%, O < 0.35%	Fe > 97.2%, C < 1.0% N < 1.0%, O < 0.4%
Nanohardness (estimation)	2.2 GPa	9.7 GPa

Table 2 Composition of three MR fluids

Name	Composition
MR fluid 1	Soft-grade MR fluid + cerium oxide
MR fluid 2	Hard-grade MR fluid + cerium oxide
MR fluid 3	Pure hard-grade MR fluid

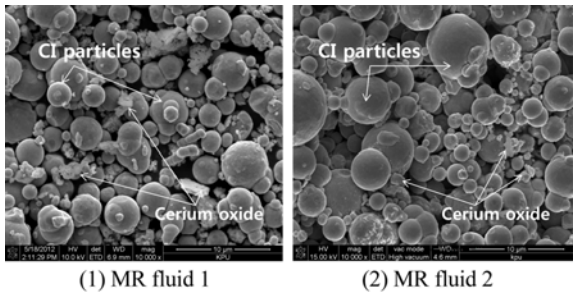

(1) MR fluid 1 (2) MR fluid 2

Fig. 2 SEM images of CI and cerium oxide particles in MR fluid

pure MR fluid without abrasives. The pure MR fluid used in this study consists of 38.2 vol% spherical carbonyl iron (CI) particles and 58.4 vol% deionized water. Additional components of 2.6 vol% glycerol and 0.8 vol% sodium carbonate assist with the stabilization of the MR fluid, as described by Jacobs.[16] Two different grades of CI particles were used, a mechanically soft-grade material and a hard-grade material. The hardness of both CI particles is estimated from the work by Shorey et al., based on the different structures and chemical compositions of the particles, which are listed in Table 1 along with other properties.[17] Abrasive cerium oxide particles, with an average particle size of 1.8

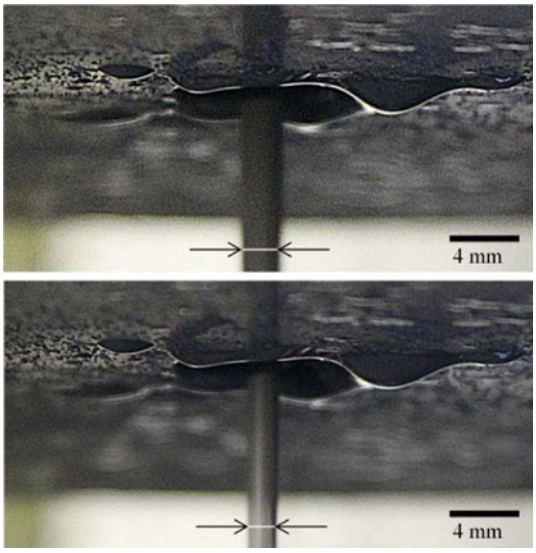

Fig. 3 Variation in jet diameter due to magnetic field (top, magnet off; bottom, magnet on)

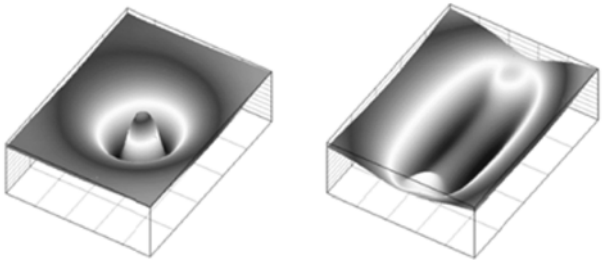

Fig. 4 Removal spot polished by a stationary (left) and a reciprocating (right) nozzle

μm, were mixed with the MR fluid at a volume ratio of 5:95. The composition of each of the three MR fluids that were prepared is listed in Table 2. Additionally, SEM images that show the CI and cerium oxide particles from MR fluids 1 and 2 were taken after drying, and are shown in Fig. 2.

2.2 MR fluid jet and material removal spotting

Fig. 3 shows the MR fluid jets leaving the electromagnet-nozzle module, both without and with the magnetic field. When the magnetic field is applied, the jet surface becomes smooth and the jet stream becomes highly collimated. Furthermore, the jet diameter decreases to 1.7 mm, which is smaller than the inner diameter of the nozzle. This is believed to be due to a solidified MR fluid layer that adheres to the nozzle edge perimeter where the magnetic field strength is highest, and thus narrows the exit diameter.

By impinging the jet perpendicularly on the BK7 samples, material removal spots are formed. Fig. 4 shows the images of typical removal spots measured by a 3D optical surface profiler (Zygo NewView 7000): On the left is with a stationary nozzle, and on the right with a nozzle that reciprocates over a small constant distance. This study focuses on the stationary removal spots in order to evaluate the material removal rates and surface roughness.

3. Material Removal Mechanism

3.1 Interaction between particles and wall

MR fluid jet finishing is modeled as an erosion process caused by the impact of the CI particles suspended in water, which creates wear on a target surface. The material removal is influenced by the size, concentration, and angularity of the particles, and by the material hardness, interstitial liquid, impact repetition, and impact angle.

Considering the small kinetic energy of the spherical CI particles and fine abrasives (below 1 nJ at the velocity of 30 m/s), the response of glass materials will be elastic or weakly plastic deformation, and the process may be regarded as ductile erosion.

In an MR fluid jet, the nature of the particle-wall interactions change from the jet impingement to the wall jet that spreads out over the target surface. In the impingement zone, the slurry becomes squeezed by the incoming jet, and the particle impacts are cushioned by this squeezed layer, so that the normal velocity is lower near the surface.[22] With a low particle kinetic energy, impact with the wall may even be prevented, causing a material removal rate close to zero at the jet center.

Along the wall surface, in the case of a low-concentration slurry, the particles impact on the surface with an impact angle that decreases away from the center. At the same time, the radial velocity increases quickly to a maximum value, and then gradually decreases along the flow streamlines. A low impact angle and high radial velocity can produce the maximum microcutting efficiency, causing a W-shaped erosion profile.[20,23] However, for a high-concentration slurry (concentrations of solid particles over 30 vol%) such as an MR fluid, the directional impacts of a single particle are not possible. The slurry layer that is squeezed out from the jet center develops along the wall, and forms a barrier layer that prevents the direct impact of the incoming particles. Therefore, the material removal in this case is due to the friction of the slurry flow along the wall surface causing a shear stress in the radial direction.

The wall shear stress is used as a measure of friction, and there are two different shear stresses that can be induced in a dense slurry: The frictional shear stress and the collisional stress caused by impacts of suspended particles. There is a viscous sublayer in the vicinity of the wall surface where turbulent fluctuations are negligible. The viscosity of this sublayer is high due to the presence of submerged fine particles, and this causes a frictional shear stress on the wall surface.[24] The collisional stress is induced on the wall by the interaction between the particles in a dense slurry, and increases with the shear rate.[25] The shearing of closely spaced particles adjacent to the wall surface will generate random collisions, and impel some particles toward the surface. These impelled particles will then generate a collisional stress that acts on the surface.

By the assumption that the rate of material removal is dependent on the shear flow of the MR fluid along the target surface, a material removal model for a high-concentration slurry can be proposed that combines the slurry erosion model and the constitutive stress equations.

3.2 Material removal model

Based on the Rabinowicz's expression for three body abrasive erosion of a surface by powdered abrasives,[26] the erosion rate can be modeled as

$$\frac{dz}{dt} = C\frac{\sigma_N v_s}{H} \tag{1}$$

where dz/dt is the material removal rate, C is a non-dimensional constant, σ_N is the normal stress acting on the surface, H is the hardness of wear surface, and v_s is the surface velocity of the particles which is identical to the wall slip velocity and given by[27]

$$v_s = \beta D\dot{\gamma}/2 \tag{2}$$

where β is the wall slip coefficient, D is the particle diameter, $\dot{\gamma}$ is the shear rate.

The normal stress in Eq. (1) will be proportional to a shear stress with a Coulomb friction coefficient and can be evaluated by Bagnold's scaling.[25,28] It presents the relationship between the normal/shear stress and the shear rate in the shear flow, by recognizing whether the internal dynamic structure of the particles is frictional or collisional. When either the solid particle concentration or the shear rate are high (grain-inertia regime), then momentum transfer through interparticle collisions primarily determines the flow behavior, and the contribution of the interstitial liquid is negligible. Therefore, collisional impacts dominate the particle-wall interaction near the wall surface. On the other hand, for relatively small shear rates or a low particle concentration (viscous regime), the frictional force by a liquid's viscosity becomes critical rather than the collisional force.

The two flow regimes are distinguished by the dimensionless Bagnold Number N, which is the ratio of collisional stresses to viscous stresses and defined as

$$N = \frac{\lambda^{0.5}\rho_p D^2\dot{\gamma}}{\eta} \tag{3}$$

where λ is the linear concentration of particles, ρ_p is the particle density, and η is the liquid viscosity.

The Bagnold number varies linearly with the shear rate and the normal stress, and marks a transition from the frictional to the collisional regimes as the Bagnold number increases. It has been identified that the stress is frictional for $N < 40$ and collisional for $N > 100$. There is a transitional range between these two values where each regime is not strictly confined.[29]

Using the Bagnold's equation for the normal stress with respect to N, the equation for the material removal rate due to an MR fluid may be taken as

$$\frac{dz}{dt} = \frac{C_1}{H}\rho_p\lambda^2 D^3\dot{\gamma}^3 \tag{4}$$

for the high shear rate with $N > 100$, and

$$\frac{dz}{dt} = \frac{C_2}{H}\lambda^{1.5}\eta D\dot{\gamma}^2 \tag{5}$$

for the low shear rate with $N < 40$, where C_1 and C_2 are non-dimensional coefficients of machinability.

It is not possible to verify in this study the dependence of the proposed model on each parameter, owing to the limited choice of material conditions for the MR fluid. Accordingly, in this study we focus on the dependence of the material removal rates on the shear. The shear rate is calculated by numerical analysis using a commercial CFD code, by assuming that the MR fluid behaves as a Newtonian fluid with a known viscosity. In order to allow a variation in the jet velocity to create different wall shear rates, Eqs. (4) and (5) will be applied and evaluated, according to the respective flow regimes.

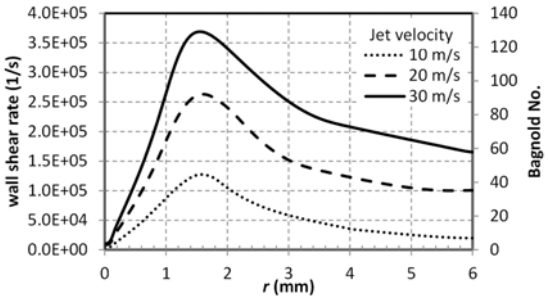

Fig. 5 Distributions of shear rate and corresponding Bagnold number along the radial distance for three jet velocities

3.3 Numerical analysis of jet flow for wall shear rate

Simulations were performed using commercial CFD software (Fluent 6.3). A multiphase volume of fluid (VOF) model was used to iteratively reach the steady-state solution. A 2D axisymmetric model space was used to simplify the calculations. The computational domain was 5 mm along the axial length (parallel to the vertical jet) and 6 mm in radial length (parallel to the workpiece surface). A rectangular mesh of nonuniform spacing was used, with minimum spacings of 48 mm and 80 mm in the axial and radial directions respectively. The total number of elements was 3600.

There is no magnetic field at the site of jet impingement and radial flow. In the absence of the magnetic field, the viscosity of the MR fluid is constant, and the MR fluid can be considered to behave like a Newtonian fluid.[30] The dynamic viscosity was measured at 110 mPa·s by a rheometer at a shear rate of 760 /s. Additionally, the Reynolds number of the jet flow in this study is 1980, and the flow is assumed to be laminar.

Fig. 5 shows the profiles of the simulated wall shear rates and the Bagnold numbers along the radial distance, for a fluid jet of 1.7 mm diameter impinging upon the target wall at velocities of 10, 20, and 30 m/s. The shear rates are zero at the center and increase linearly until they reach their peak values at about r=1.6 mm, which is approximately the same for all three jet velocities. The changes of the shear rates with radius, including the linear increase and subsequent approximately power-law decay, agree with the results from the literature regarding a laminar jet impinging on a solid surface.[31] At the jet velocity of 10 m/s the Bagnold numbers mostly remain under 40. At 20 and 30 m/s, the Bagnold numbers for a large radial region are in the range corresponding to the transitional and grain-inertia regimes, except for the region inside the jet radius ($r < 0.85$ mm).

4. Results and Discussion

4.1 Removal depth profiles of stationary spots

Material removal depth profiles $h(r)$ (=-$z(r)$) were obtained from the

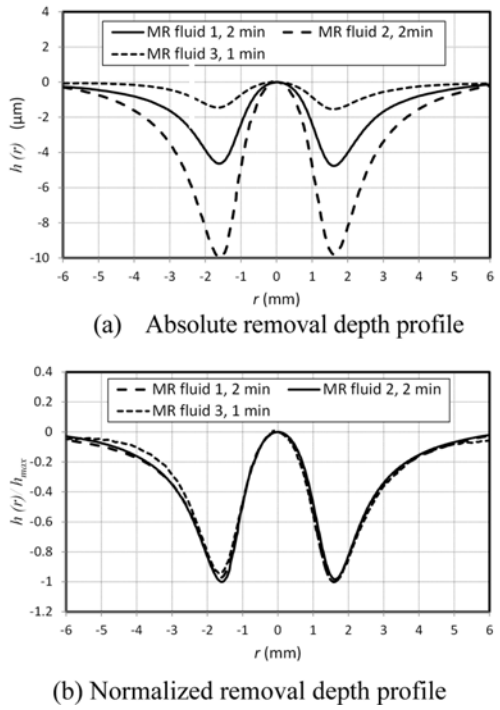

Fig. 6 Material removal profiles from the MR fluid 1, 2, and 3

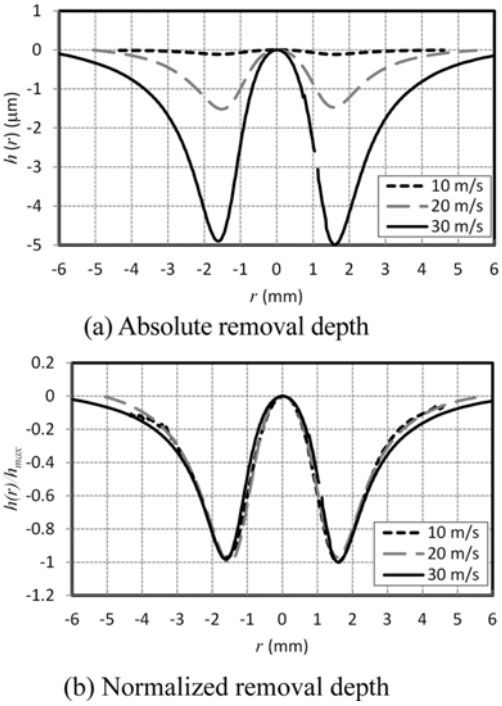

Fig. 8 Material removal depth as a function of the distance r from the jet center, three jet velocities with MR fluid 2

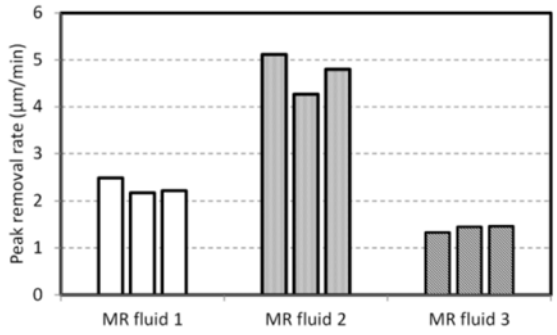

Fig. 7 Peak material removal rate variation with MR fluid

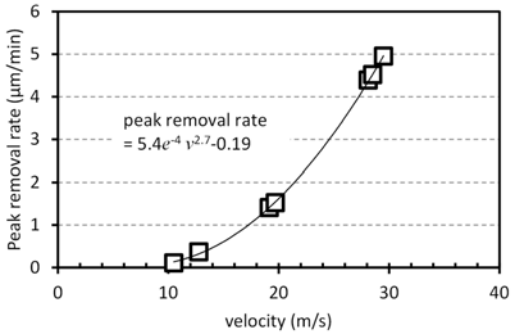

Fig. 9 Peak removal rate with the normal jet velocity

3D optical image of the stationary nozzle removal spot on the BK7 specimen surface. First, the effect of the different compositions of the MR fluid was analyzed. Fig. 6 shows the absolute and normalized ($-h(r)/h_{max}$) removal depths for each of the three MR fluids, with the constant jet velocity of 30 m/s and different removal durations: 2 min for MR fluid 1 and 2, and 1 min for MR fluid 3.

The removal depth varies with the composition of the MR fluid and the processing duration, but the general removal behavior is the same for all MR fluids from the normalized graph, with peak removal positions located at r=1.6 mm, which agrees with the position of the maximum wall shear rates in Fig. 5.

Fig. 7 compares the peak removal rate in the jet-polished spots for the three MR fluids, with the experiment repeated three times for each MR fluid. The two MR fluids that contain cerium oxide are able to remove glass faster than the pure MR fluid. Owing to the synergy between the cerium oxide particles and the hard-grade CI particles, which are harder than the BK7 glass, MR fluid 2 demonstrates the highest peak removal rate.

The distributions of material removal rate are constant with respect to repeated experiments with all MR fluids, which validates the modeling of MR fluid with abrasives as a monodisperse particle slurry. It can also be determined that the W-shaped profiles are related to the flow field over the wall surface.

Fig. 8 shows the removal depth profiles and their normalized plots for jet velocities of 10, 20, and 30 m/s using MR fluid 2. As the jet velocity increases the removal depth becomes deeper and this trend can also be seen in Fig. 9, which shows the peak removal rate for multiple experiments at different jet velocity,[32] describing a power law with an exponent of 2.7. Although it appears from Fig. 8(a) that the W-shaped profile becomes wider with the jet velocity, the normalized distributions of material removal rate show only a small difference in Fig. 8(b), maintaining the same peak removal position as was previously seen in Fig. 6.

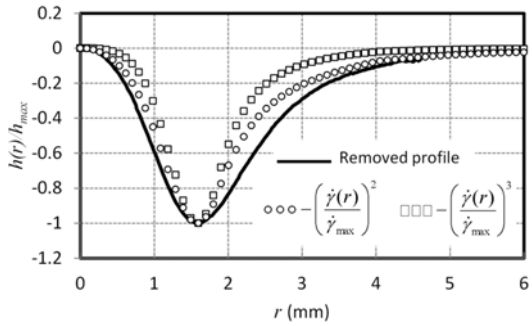

Fig. 10 Normalized material removal distributions by experiment and theoretical model, for jet velocity of 10 m/s

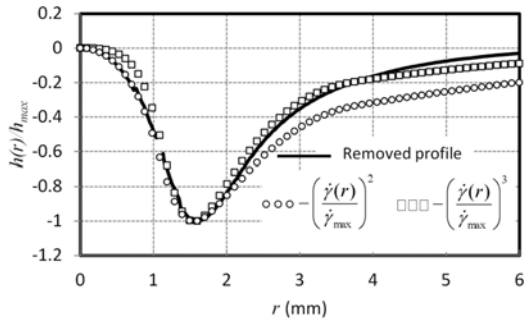

Fig. 11 Normalized material removal distributions by experiment and theoretical model, for jet velocity of 30 m/s

4.2 Comparison between modeling and experimental results

In this section we validate the material removal models for both the stress regimes. The wall shear rate distributions $\dot{\gamma}(r)$ for jet velocities of 10 and 30 m/s were applied to Eqs. (4) and (5), and then both equations were normalized with respect to their maximum values. In Figs. 10 and 11, the normalized quantities $(\dot{\gamma}(r)/\dot{\gamma}_{max})^2$ and $(\dot{\gamma}(r)/\dot{\gamma}_{max})^3$ are shown together with a normalized experimental removal rate. The experimental line is the average of two experiments at the same radial distance from the jet center, taking into account the radial symmetry of the system.

When the jet velocity is 10 m/s, as shown in Fig. 10, the frictional stress may be dominant in the shear flow over the surface, as inferred from the small Bagnold number in Fig. 5. The material removal model using the frictional normal stress with a low shear rate is close to the experimental distribution, with the same peak removal position, although there is a slight deviation at r=2~3 mm. The removal model using the collisional stress shows a steeper change with the radial distance near to the peak position.

Fig. 11 presents the results at the jet velocity of 30 m/s. In contrast to Fig. 10, the removal model based on the collisional stress agrees well with the experimental result, except for near the center where the shear rate is low. Even though the experimental distributions of material removal rate are similar for jet velocities up to 30 m/s, the dependence on the shear rate is quite different between 10 to 30 m/s, because the mutual dynamic behavior between the particles inside the shear flow transitions from frictional to collisional. Therefore, the constitutive relations of the normal stress that acts on the surface change. Eventually, this transition may cause a rapid increase in the peak removal rate with the jet velocity at higher velocity conditions, which was expressed with the power-law fit of the peak removal rate with respect to the jet velocity in Fig. 9.

When the jet velocity was increased further (e.g., over 40 m/s), additional erosive removal at the jet center appeared, due to the increased energy of the jet in the direction normal to the specimen surface. This changes the removal depth and invalidates the assumption that the material removal occurs by the shear flow along the surface.

4.3 Surface texture and roughness

Fig. 12 shows the surface textures of a 70 mm × 50 mm area at the center (1), the deepest removal point (2), and the edge (3) of a removal spot, obtained by applying MR fluid 2 with jet velocities of 10 and 30 m/s. The initial surface roughness of the pitch-polished BK7 glass disks (as-received) was 1.15 nm *rms* and 18.5 nm *Rp-v*.

The surface textures that are generated by an impinging jet velocity of 10 m/s appear similar irrespective of the position in the removal spot. The surface roughness values are 1.3/23.7 nm, 1.3/25.8 nm, and 1.2/20.9 nm (*rms*/*Rp-v*) at 1, 2, and 3, respectively. At the jet velocity of 30 m/s, because of the increased force of the particles, the random craters are more visible, but the increase of the surface roughness is negligible at 1.4/26.4 nm, 3.3/56.6 nm, and 1.3/30.0 nm at the same positions.

Although there is little material removal at the center of the spot, the surface has been deformed with multiple indentation marks, which are more distinct at the jet velocity of 30 m/s. These are assumed to be caused by the indentation of large particles without a tangential velocity. At the deepest position, the surface roughness increases at both jet velocities, but a wavy pattern is generated along the radial direction at 30 m/s jet. This ripple formation is a phenomenon that occurs on the surface of a ductile material which is subjected to low-angle impact erosion by solid particles, and occurs by micro-cutting or micro-ploughing.[33] The ripples form at the deepest area of removal and become more severe as the peak removal depth increases. They did not occur at jet velocities of 10-20 m/s, or when the nozzle was moved with a reciprocating motion. Therefore, the ripples here seem to be due to the following reason: In addition to the horizontal velocity over the surface, the collisional impact between the particles under high shear rate causes some impacts at an angle to the surface, at the area of deepest erosion. At the edge of the removal spot, many nanocraters are observed. The surface roughness values are similar to those at the center, but the surface textures appear visually different to those at the center.

5. Conclusion

MR fluid jet polishing is a material removal process that uses the impingement of a collimated stream of high-concentration slurry onto a target surface. From the experiments with a BK7 glass specimen, it was identified that the absolute material removal depths varied with the type of MR fluid (hardness of CI particles and presence of abrasives), the processing duration, and the impinging jet velocity, but that the normalized spatial distribution of the material removal rate was relatively unchanged.

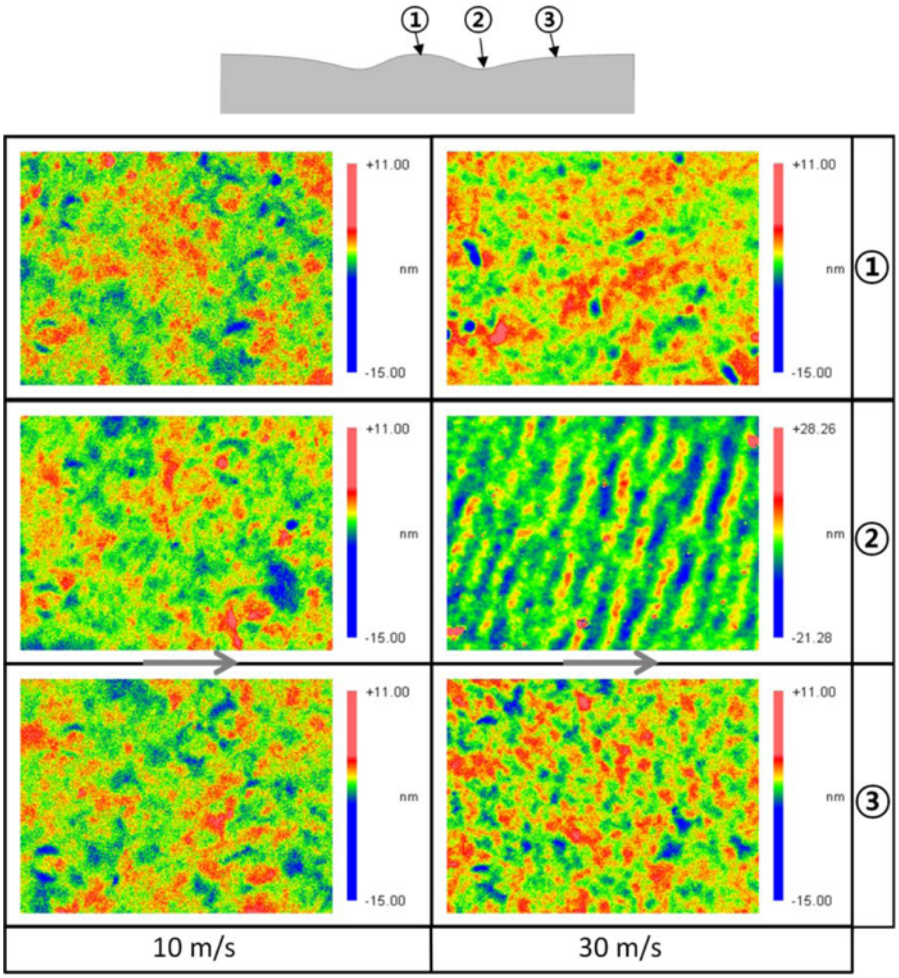

Fig. 12 Surface roughness at the center, area of deepest erosion, and edge of the axisymmetric spot

Under the low jet velocities (10~30 m/s), direct impact of the particles from the free jet to the target surface in the impingement region is almost impossible, because the MR fluid slurry forms a barrier layer as it is squeezed beneath the incoming jet. The material removal is subsequently caused by the tangential flow along the specimen surface, and a W-shaped removal spot is formed with zero material removal at the jet center, in the situation with a stationary nozzle.

Material removal by the MR fluid flowing over the specimen surface is modeled by the combination of the wear model for slurry erosion and the constitutive stress equation from granular flow theory.

Different stress regimes were identified with an increase of the jet velocity from 10 to 30 m/s, which are differentiated by the Bagnold number. This takes into account the material properties and the wall shear rates, which are obtained by CFD simulations of the flow field along the target surface. At a jet velocity of 10 m/s, the frictional stress dominates in a sublayer at the wall, which behaves like a single-phase fluid, and the material removal rate is proportional to the square of the wall shear rate. Conversely, the collisional stress dominates at the jet velocity of 30 m/s owing to the increased wall shear rate, causing the material removal rate to be proportional to the third power of the shear rate. Each model approximation agrees with the normalized removal profiles measured by experiment, at the relevant jet velocity and position.

The surface topographies inside the polished spot show irregular patterns due to cutting and ploughing at the nanometer scale. Local textures in the W-shaped spot are different at the center, area of deepest erosion, and edge, especially at a jet velocity of 30 m/s, which exhibits both the frictional and collisional regimes. The change of the surface roughness with the jet velocity was negligible in tested experiments, with approximate values of 1.3 nm *rms* and 30 nm *Rp-v*.

Because of the limited capacity to alter the material conditions, the current study was limited in the ability to verify the suggested removal models over a wide range of parameter conditions. Nevertheless, it is believed that this work could provide insight into the mechanisms of material removal by a high concentration slurry for fine finishing of precision parts, and in particular for the case of impingement by an MR fluid jet.

ACKNOWLEDGEMENT

This research was supported by Basic Science Research Program through the National Research Foundation of Korea(NRF) funded by the Ministry of Education, Science and Technology(No.Grant Number: 2010-0004018)

REFERENCES

1. Fähnle, O. W., Brug, H. V., and Frankena, H. J., "Fluid Jet Polishing of Optical Surfaces," Applied Optics, Vol. 37, No. 28, pp. 6771-6773, 1998.
2. Jafar, R. H. M., Spelt, J., and Papini, M., "Surface Roughness and Erosion Rate of Abrasive Jet Micro-Machined Channels: Experiments and Analytical Model," Wear, Vol. 303, No. 1, pp. 138-145, 2013.
3. Slikkerveer, P., Bouten, P., and De Haas, F., "High Quality Mechanical Etching of Brittle Materials by Powder Blasting," Sensors and Actuators A: Physical, Vol. 85, No. 1, pp. 296-303, 2000.
4. Finnie, I., "Erosion of Surfaces by Solid Particles," Wear, Vol. 3, No. 2, pp. 87-103, 1960.
5. Hutchings, I. M., "Ductile-Brittle Transitions and Wear Maps for the Erosion and Abrasion of Brittle Materials," Journal of Physics D: Applied Physics, Vol. 25, No. 1A, pp. A212-A221, 1992.
6. Buijs, M. and Pasmans, J., "Erosion of Glass by Alumina Particles: Transitions and Exponents," Wear, Vol. 184, No. 1, pp. 61-65, 1995.
7. Bousser, E., Martinu, L., and Klemberg-Sapieha, J., "Effect of Erodent Properties on the Solid Particle Erosion Mechanisms of Brittle Materials," Journal of Materials Science, Vol. 48, No. 16, pp. 5543-5558, 2013.
8. Verspui, M. A., Slikkerveer, P. J., Skerka, G. J. E., Oomen, I., and de With, G., "Validation of the Erosion Map for Spherical Particle Impacts on Glass," Wear, Vol. 215, No. 1, pp. 77-82, 1998.
9. Wensink, H., Schlautmann, S., Goedbloed, M. H., and Elwenspoek, M. C., "Fine Tuning the Roughness of Powder Blasted Surfaces," Journal of Micromechanics and Microengineering, Vol. 12, No. 5, pp. 616-620, 2002.
10. Jafar, R. H. M., Spelt, J. K., and Papini, M., "Numerical Simulation of Surface Roughness and Erosion Rate of Abrasive Jet Micro-Machined Channels," Wear, Vol. 303, No. 1, pp. 302-312, 2013.
11. Liu, H., Wang, J., and Huang, C., "Abrasive Liquid Jet as a Flexible Polishing Tool," International Journal of Materials and Product Technology, Vol. 31, No. 1, pp. 2-13, 2008.
12. Sooraj, V. and Radhakrishnan, V., "Elastic Impact of Abrasives for Controlled Erosion in Fine Finishing of Surfaces," Journal of Manufacturing Science and Engineering, Vol. 135, No. 5, Paper No. 051019, 2013.
13. Kordonski, W., Shorey, A., and Tricard, M., "Precision Finishing with Magnetorheological (MR) Jet Technology," Proc. of SPIE, Vol. TD03, pp. 1-3, 2005.
14. Kordonski, W. I., Shorey, A. B., and Tricard, M., "Magnetorheological Jet (MR JetTM) Finishing Technology," Journal of Fluids Engineering, Vol. 128, No. 1, pp. 20-26, 2006.
15. Kordonski, W. I. and Jacobs, S. D., "Magnetorheological Finishing," International Journal of Modern Physics B, Vol. 10, No. 23-24, pp. 2837-2848, 1996.
16. Jacobs, S. D., "MRF with Adjustable pH," Proc. of SPIE, Vol. 8169, 2011.
17. Shorey, A. B., Kwong, K. M., Johnson, K. M., and Jacobs, S. D., "Nanoindentation Hardness of particles Used in Magnetorheological Finishing (MRF)," Applied Optics, Vol. 39, No. 28, pp. 5194-5204, 2000.
18. Sidpara, A. and Jain, V. K., "Experimental Investigations into Surface Roughness and Yield Stress in Magnetorheological Fluid based Nano-Finishing Process," Int. J. Precis. Eng. Manuf., Vol. 13, No. 6, pp. 855-860, 2012.
19. Kim, W. B., Lee, S. H., and Min, B. K., "Surface Finishing and Evaluation of Three-Dimensional Silicon Microchannel using Magnetorheological Fluid," Journal of Manufacturing Science and Engineering, Vol. 126, No. 4, pp. 772-778, 2004.
20. Beaucamp, A., Namba, Y., and Freeman, R., "Dynamic Multiphase Modeling and Optimization of Fluid Jet Polishing Process," CIRP Annals-Manufacturing Technology, Vol. 61, No. 1, pp. 315-318, 2012.
21. Gnanavelu, A., Kapur, N., Neville, A., Flores, J., and Ghorbani, N., "A Numerical Investigation of a Geometry Independent Integrated Method to Predict Erosion Rates in Slurry Erosion," Wear, Vol. 271, No. 5, pp. 712-719, 2011.
22. Clark, H. M. and Burmeister, L., "The Influence of the Squeeze Film on Particle Impact Velocities in Erosion," International Journal of Impact Engineering, Vol. 12, No. 3, pp. 415-426, 1992.
23. Turenne, S., Fiset, M., and Masounave, J., "The Effect of Sand Concentration on the Erosion of Materials by a Slurry Jet," Wear, Vol. 133, No. 1, pp. 95-106, 1989.
24. Matoušek, V., "Research Developments in Pipeline Transport of Settling Slurries," Powder Technology, Vol. 156, No. 1, pp. 43-51, 2005.
25. Hunt, M. L., Zenit, R., Campbell, C. S., and Brennen, C. E., "Revisiting the 1954 Suspension Experiments of RA Bagnold," Journal of Fluid Mechanics, Vol. 452, pp. 1-24, 2002.
26. Rabinowicz, E., Dunn, L. A., and Russell, P. G., "A Study of Abrasive Wear under Three-Body Conditions," Wear, Vol. 4, No. 5, pp. 345-355, 1961.
27. Jana, S. C., Kapoor, B., and Acrivos, A., "Apparent Wall Slip Velocity Coefficients in Concentrated Suspensions of Noncolloidal Particles," Journal of Rheology, Vol. 39, No. 6, pp. 1123-1132, 1995.
28. Bagnold, R. A., "Experiments on a Gravity-Free Dispersion of Large Solid Spheres in a Newtonian Fluid under Shear," Proc. of the Royal Society of London A: Mathematical, Physical and Engineering Sciences, Vol. 225, pp. 49-63, 1954.
29. Coussot, P. and Ancey, C., "Rheophysical Classification of Concentrated Suspensions and Granular Pastes," Physical Review E, Vol. 59, No. 4, pp. 4445-4457, 1999.
30. Engin, T., Evrensel, C., and Gordaninejad, F., "Numerical Simulation

of Laminar Flow of Water-based Magneto-Rheological Fluids in Microtubes with Wall Roughness Effect," International Communications in Heat and Mass Transfer, Vol. 32, No. 8, pp. 1016-1025, 2005.

31. Kristiawan, M., Meslem, A., Nastase, I., and Sobolik, V., "Wall Shear Rates and Mass Transfer in Impinging Jets: Comparison of Circular Convergent and Cross-Shaped Orifice Nozzles," International Journal of Heat and Mass Transfer, Vol. 55, No. 1, pp. 282-293, 2012.
32. Kim, W. W. and Kim, W. B., "Machining Performance of Optical Glass with Magnetorheological Fluid Jet Polishing," J. Korean Soc. Precis. Eng., Vol. 28, No. 8, pp. 929-935, 2011.
33. Stachowiak, G. W. and Batchelor, A. W., "Engineering Tribology," Butterworth-Heinemann, pp. 483-523, 2001.